# MONOTONIC AND CYCLIC DEFORMATION BEHAVIOR OF α-PHASE Ti-Al ALLOYS

H. M. Kim*, H. G. Paris+, and J. C. Williams*

*Carnegie-Mellon University, Pittsburgh, PA, U.S.A.

+Alcoa Laboratories, Pittsburgh, PA, U.S.A.

## Introduction

The monotonic deformation of α-phase Ti-Al alloys has been the subject of many investigations over the past two decades, and it is now well known that increasing Al content increases the tendency for planar slip in this alloy[1-4]. As a result of fairly recent single crystal studies by Paton et al[5], this subject is now better understood. They determined the temperature and composition dependence of the critical resolved shear stress (CRSS) for each of the slip systems. Their CRSS results for basal or prism slip with an $\bar{a}$ slip vector and for $\bar{c}+\bar{a}$ slip tested in Ti-6.6 wt%Al+ show that $\bar{a}$ slip is preferred to $\bar{c}+\bar{a}$ and that $\bar{a}$ slip on (0001) is only slightly more difficult than on $\{10\bar{1}0\}$. In contrast with this reasonably complete understanding of monotonic deformation, there has been essentially no work on the cyclic deformation of α-phase Ti-Al alloys.

The present investigation was designed to characterize the monotonic and cyclic deformation structures of α-phase Ti-Al alloys, especially using transmission electron microscopy (TEM). We have particularly studied how Al affects the monotonic and cyclic deformation behavior, and have compared the deformed structures typical of monotonic and cyclic loading.

## Experimental

Two alloys having different Al contents were chosen to study the effect of Al content on the deformation behavior: Ti-4%Al and Ti-8%Al. These alloys were supplied as hot rolled plates by Titanium Metals Corporation of America. The chemical compositions of these alloys are given in Table 1. Monotonic and cyclic loading specimens with 6.5mm diameter gage sections were cut with their loading directions along both the longitudinal and transverse directions of the plates. It has been found that the deformation modes and yield strengths are comparable in both loading directions. Such lack of directionality suggested a basal pole texture normal to the rolling plane, thus through-thickness compressive specimens were also tested. This latter loading condition enforces c-axis compression of many grains and either twinning or $\bar{c}+\bar{a}$ slip is expected[1].

All the specimens were heat treated in a dynamic vacuum of $1 \times 10^{-6}$ torr to provide a uniform final grain size of 40μ. The Ti-8%Al alloy was subsequently re-solution-treated in the α-phase region for 30 minutes and water-quenched to prevent formation of the ordered $\alpha_2$ ($Ti_3Al$) precipitates.

---

+All alloy compositions are given in wt% unless otherwise stated.

Controlled amounts of strain were introduced by monotonic tensile loading of the tensile specimens or by compressive loading the through-thickness specimens. Total strain-controlled fully reversed (R = -1) cyclic tests (low cycle fatigue tests) were conducted at room temperature with a 50-kip closed-loop, servo-controlled hydraulic MTS test system. Woods metal grips were used to insure proper axial alignment of the specimens and constant strain rate of 0.01 $sec^{-1}$ was used throughout all the fatigue tests.

The nature of the monotonically and cyclically induced deformation structures was studied by both light and transmission electron microscopy. Thin foils were prepared by the window method as has been previously described in detail elsewhere[5].

## Results and Discussion

### 1. Monotonic Deformation

Dislocation structures typical of the early stages of tensile deformation ($\varepsilon_p \simeq 0.3\%$) are shown in Figure 1. At this low strain, little difference in dislocation structures between Ti-4Al and Ti-8Al generally was found; both alloys contained heterogeneously distributed slip bands during the early stages of monotonic deformation. Even at this 0.3% strain, some grains showed more homogeneous dislocation arrangements in Ti-4Al. This suggests that some grains have undergone strains as high as several times the average macroscopic strain. Further, within some grains the dislocation densities varied locally, probably due to different accommodation requirements from different neighboring grains. Prism slip with an $\bar{a}$ slip vector is the principal deformation mode in this stage and very few $\bar{c}+\bar{a}$ dislocations and twins are observed. This observation agrees well with the earlier single crystal results[6] which showed that prism slip has the lowest CRSS at room temperature.

Although similar dislocation structures are observed during the initial deformation stage, quite large differences between Ti-4Al and Ti-8Al are seen after larger amounts of plastic deformation. Thin foil micrographs of these alloys after heavier deformation ($\varepsilon_p \simeq 3.6\%$) in tension are shown in Figure 2. Prism slip with an $\bar{a}$ slip vector is still the main deformation mode at these strains. In Ti-4Al, a homogeneous distribution of dislocations is typically observed, although poorly developed planar slip can be observed in grains viewed along [0001], i.e. so that the prism planes are seen on edge. Such local variations are due to the anistropic nature of deformation in this hcp alloy. Similar observations have previously been made by others[1,2]. In contrast, well defined slip bands are seen in Ti-8Al in all orientations. Thus, the effect of increasing Al content is not only to change the slip character from wavy to planar but also to cause the bands of planar slip to become more constricted and better defined. That is, more inhomogeneous slip distribution or strain localization occurs in the higher Al alloys.

Very few $\bar{c}+\bar{a}$ dislocations are observed in the early stages of deformation of the longitudinal and transverse specimens. However, numerous $\bar{c}+\bar{a}$ dislocations are observed in both alloys strained in through-thickness compression (Fig. 3). In general, the density of $\bar{c}+\bar{a}$ dislocations was higher in Ti-8Al than in Ti-4Al at comparable plastic strains. The distribution of $\bar{c}+\bar{a}$ dislocations in Ti-8Al also appears to be more homogeneous than in Ti-4Al

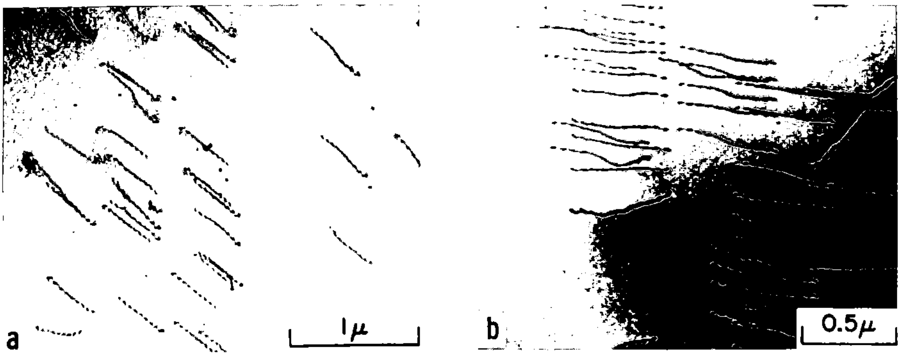


Fig. 1 - Monotonic deformation structures after $\varepsilon_p \simeq 0.3\%$
a) Ti-4Al b) Ti-8Al.

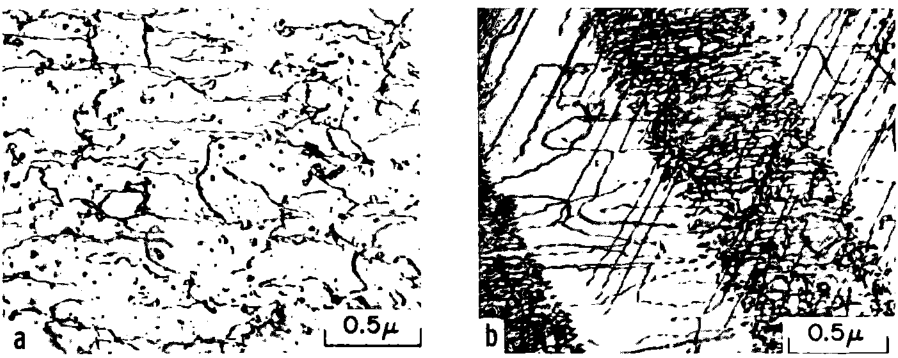


Fig. 2 - Monotonic deformation structures after $\varepsilon_p \simeq 3.6\%$
a) Ti-4Al b) Ti-8Al

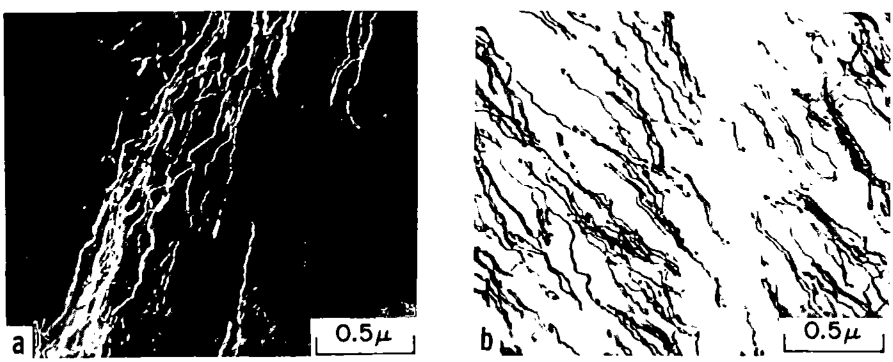


Fig. 3 - $\bar{c}+\bar{a}$ dislocations after $\varepsilon_p \simeq 3.6\%$
a) Ti-4Al b) Ti-8Al

as shown in Figure 3, although some caution needs to be exercised in making this judgment in polycrystals because the relative orientations of the foil and the slip plane are not known. Thus, when the active slip plane is seen in plan view the dislocations can appear homogeneously distributed even though they are arranged in discrete bands. The $\bar{c}+\bar{a}$ dislocations are predominantly edge in character,whereas most of the $\bar{a}$ dislocations are screw in characters. The higher density of $\bar{c}+\bar{a}$ dislocations in the Ti-8Al is consistent with the virtual absence of twinning. Thus all c-axis component deformation must be accommodated by $\bar{c}+\bar{a}$ slip in this alloy,whereas some is accommodated by twinning in Ti-4Al.

Twinning is the alternative to $\bar{c}+\bar{a}$ slip as a c-axis deformation mode of α-Titanium. In the Ti-4Al alloy, twinning was fairly common, whereas it was quite limited in extent in Ti-8Al. Optical microscopy was used to measure the twin volume fractions for various monotonic deformations. These data are seen in Table 2, and they show that increasing Al tends to suppress the occurrence of twinning. Since most grains were oriented with the c-axis normal to the plane of the plate, twins observed in the tensile specimens were the result of accommodation of the through-thickness contraction. On the other hand, twins in the through-thickness compression were the result of direct accommodation of the applied strain. As a result, twinning was always less extensive in longitudinal tension than in through-thickness compression. For example, in Ti-8Al twinning was not observed after tensile strain of 3.6%, whereas some twins were seen after a through-thickness compressive strain of 3.6%.

2. Cyclic Deformation

Since both Ti-4Al and Ti-8Al alloys do not show any saturation stages during cyclic straining, most of the dislocation arrangements described below have been obtained after visible cracks have appeared. Thus, the following micrographs, unless otherwise stated, show the cyclically deformed structures of the bulk material when the fatigue cracks are initiated. Cyclic deformation modes were found to be the same as monotonic deformation modes. That is, $\bar{a}$ slip, $\bar{c}+\bar{a}$ slip and twinning were observed in all of the cyclically deformed conditions of both alloys, but the extent of each of these was much higher than after a corresponding amount of monotonic deformation.

$\bar{a}$ slip

The dominant deformation mode in the LCF specimens was a slip on prism planes as in monotonic deformation. Typical arrangements of dislocations with $\bar{a}$ Burgers vectors are shown in Figures 4 and 5. The detailed configurations of dislocations after cyclic deformation differ from that in the monotonically deformed samples in the following ways. First, while samples of Ti-4Al contain homogeneously distributed dislocations, most of which are long straight screws, the dislocations in the cyclically deformed samples are not so straight and thus are not in pure screw orientation (Fig. 4(a)). This difference probably reflects the incomplete reversibility of dislocation motion during fully reversed loading in LCF. In the cyclically deformed Ti-8Al, inhomogeneous banded dislocations are seen (Fig. 5). The major difference in these bands is the amount of dislocation debris present after cyclic loading. This may again result from incomplete slip reversibility. This is especially true at low strain amplitudes. Figures 4(a) and 5(a) show

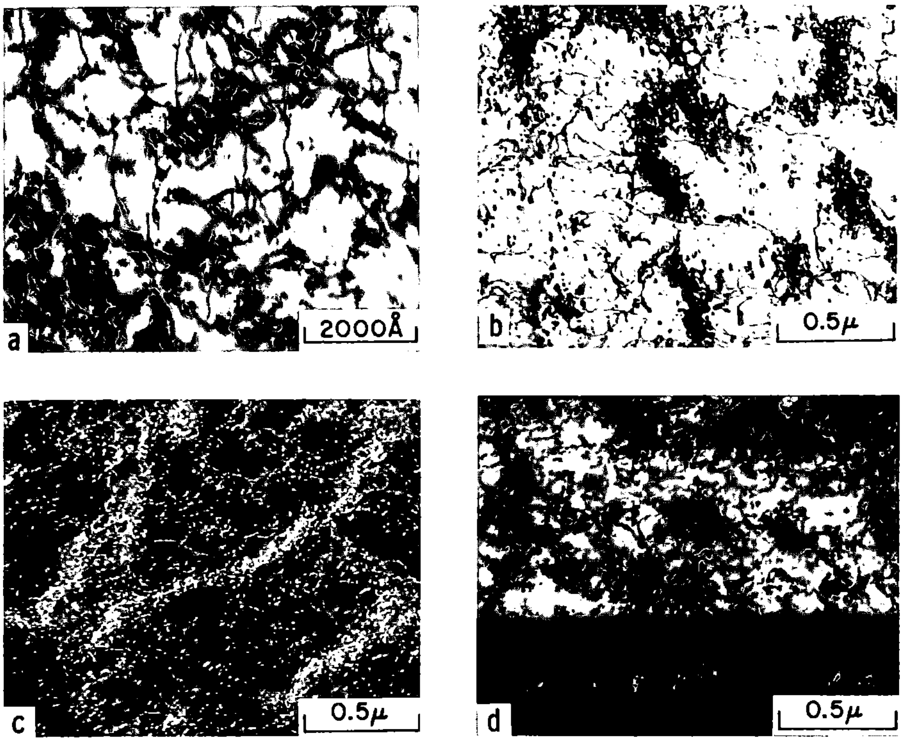


Fig. 4 - Cyclic deformation structures in Ti-4Al

a) $\frac{\Delta\varepsilon_T}{2} = 0.5\%$ b) $\frac{\Delta\varepsilon_T}{2} = 1\%$ c) $\frac{\Delta\varepsilon_T}{2} = 2\%$ d) $\frac{\Delta\varepsilon_T}{2} = 3\%$

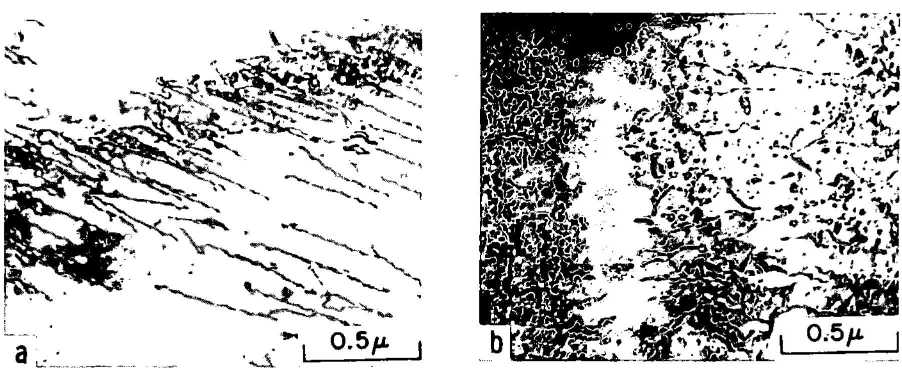


Fig. 5 - (caption on next page)

the dislocation structures of Ti-4Al and Ti-8Al, respectively, at $\frac{\Delta\varepsilon_T}{2} = 0.5\%$. It may be desirable to compare these micrographs with those obtained after 0.3% of tensile plastic strain (Fig. 1). When this is done, it can be seen that the dislocation arrangements in Ti-4Al are more significantly altered by cyclic loading at low strain amplitudes than in Ti-8Al. Thus, low amplitude cyclic straining of Ti-8Al leads to dislocation arrangements that are more comparable to monotonic loading although subtle differences exist.

At higher strain amplitudes ($\frac{\Delta\varepsilon_T}{2} = 1\%$) the cyclically loaded Ti-4Al shows homogeneously distributed dislocation tangles, extensive dislocation debris, especially dislocation loops, and the early stages of cell formation (Fig. 4(b)). It has been observed that these cells mainly consist of dislocation loops. The variation in dislocation arrangements is nearly as great from grain to grain as it is between small differences in cyclic strain amplitude. This is not surprising because the lower symmetry of α-phase leads to a larger Taylor factor and thus larger variations in effective strain from grain to grain.

Cellular structures are also observed in Ti-4Al at $\frac{\Delta\varepsilon_T}{2} = 2\%$ (Fig. 4(c)) and at $\frac{\Delta\varepsilon_T}{2} = 3\%$ (Fig. 4(d)). Figure 4(d) shows poorly developed cellular structures and a twin whose $K_1$ plane has been found to be $(10\bar{1}2)$. Figure 4(d) shows the high density of dislocations along the twin-matrix interface. At even higher strain amplitudes ($\frac{\Delta\varepsilon_T}{2} > 3\%$) in Ti-4Al, instabilities of test specimens are developed during cycling and very high densities of twinning and tangled dislocations are observed.

Cyclic deformation structures in Ti-8Al at $\frac{\Delta\varepsilon_T}{2} = 1\%$ are shown in Figure 5(b). Much higher densities of dislocations are observed than at $\frac{\Delta\varepsilon_T}{2} = 0.5\%$ (Fig. 5(a)) and the dislocation free zones between slip bands become narrower. Dislocations in slip bands are no longer straight and a high density of debris is noted. As the applied strain amplitude is increased, more slip bands appear and the dislocation free zones between slip bands tend to disappear. That is, at high strain amplitudes the distribution of dislocations becomes more homogeneous although intense slip bands are still present, but these are superimposed on the homogeneous dislocation distribution, as shown in Figures 5(c) and (d).

Some thin foils of Ti-4Al were prepared after interrupting fatigue cycling. Figure 6(a) shows deformed structures after 10 cycles at $\frac{\Delta\varepsilon_T}{2} = 1\%$. This interruption corresponds to the onset of cyclic softening which follows the initial cyclic hardening. Cyclic softening after 10 cycles continues until the specimen breaks by fatigue failure. A high density of homogeneously distributed dislocations is observed and no cellular structures like those after failure of the specimen can be seen. This indicates that cellular structures are developed during cyclic softening. Figure 6(b) shows dislocation structures after 1.5 cycles at $\frac{\Delta\varepsilon_T}{2} = 5\%$. Here, too, homogenous arrays of dislocation tangles are seen but no cell formation can be found. These observations suggest that cellular structures are not developed during cyclic hardening[7]. Finally, most straight segments of the $\bar{a}$ dis-

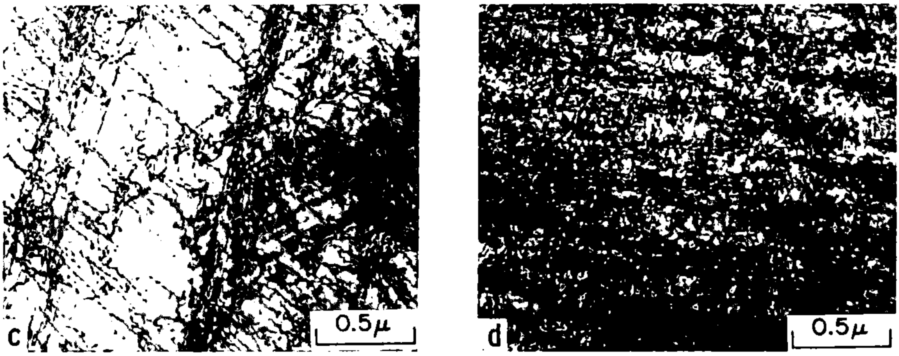


Fig. 5 - Cyclic deformation structures in Ti-8Al

a) $\frac{\Delta\varepsilon_T}{2} = 0.5\%$ b) $\frac{\Delta\varepsilon_T}{2} = 1\%$ c) $\frac{\Delta\varepsilon_T}{2} = 1.5\%$ d) $\frac{\Delta\varepsilon_T}{2} = 3\%$

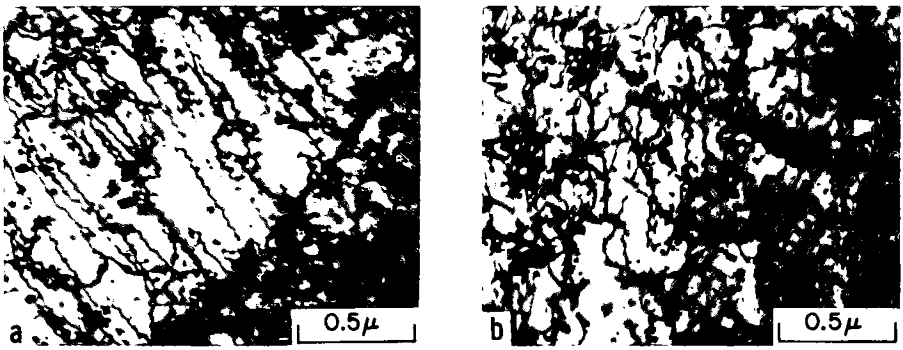


Fig. 6 - Cyclic deformation structures in Ti-4Al

a) after 10 cycles at $\frac{\Delta\varepsilon_T}{2} = 1\%$ b) after 1-1/2 cycles at $\frac{\Delta\varepsilon_T}{2} = 5\%$

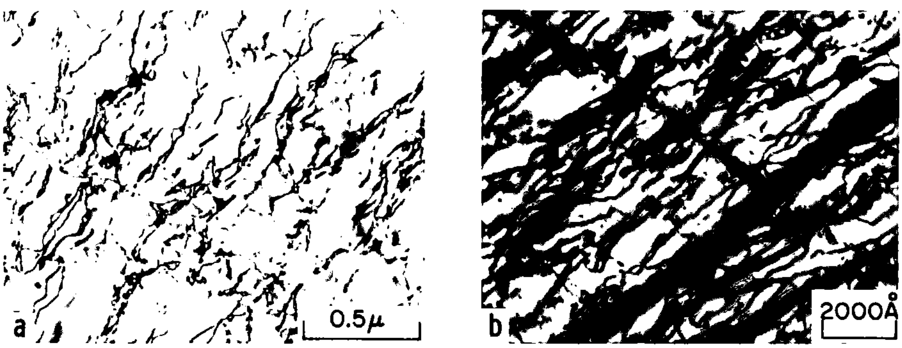


Fig. 7 - $\bar{c}+\bar{a}$ dislocations after cyclic deformation

a) Ti-4Al, $\frac{\Delta\varepsilon_T}{2} = 0.5\%$ b) Ti-8Al, $\frac{\Delta\varepsilon_T}{2} = 1.5\%$

locations observed after deformation lie in screw orientation. The differences in slip character between monotonic and cyclic deformations are summarized in Tables 3 and 4.

$\bar{c}+\bar{a}$ slip

Under all cyclic loading conditions (both Ti-4Al and Ti-8Al), even at low strain amplitudes, $\bar{c}+\bar{a}$ slip is found in some grains. This is consistent with the generally higher dislocation density in cyclically deformed materials. Thus, the effective strain is higher in cyclic loading than in monotonic loading as judged by dislocation density. We suggest that this may reflect poor local slip reversibility so that new dislocations are generated during reverse straining. The result of this is to increase the dislocation density in cyclically loaded specimens compared to comparable strains in monotonic loading. Figure 7(a) shows $\bar{c}+\bar{a}$ dislocations in Ti-4Al at $\frac{\Delta\varepsilon_T}{2} = 1.5\%$. Residual contrast from $\bar{a}$ dislocations on prism slip planes also is seen in Figure 7(b). Generally, all $\bar{c}+\bar{a}$ dislocations observed after cyclic deformation have the following characteristics, except those which accommodate twinning shear: 1) they are in edge orientation; 2) only one slip system of $\bar{c}+\bar{a}$ slip is observed with one grain; 3) very little dislocation debris with $\bar{c}+\bar{a}$ Burgers Vectors is found, and 4) higher densities are observed in somewhat more homogeneous arrays. Among these, 1), 2) and 3) are similar to monotonic deformation, but 4) is characteristic of cyclic deformation.

The above observations help explain why the dislocation debris found only consists of $\bar{a}$ Burgers Vectors. When $\bar{c}+\bar{a}$ dislocations with edge character are intersected by $\bar{a}$ dislocations with screw characters (recall that most of the straight $\bar{a}$ dislocations are in screw orientation),jogs with edge orientation are formed on the $\bar{c}+\bar{a}$ dislocations[8]. These jogs are glissile and can glide along with the $\bar{c}+\bar{a}$ dislocations or can move non-conservatively along the length of the $\bar{c}+\bar{a}$ dislocations and vanish. Thus, no dipoles and resulting dislocation loops are formed. However, in the grains where no $\bar{c}+\bar{a}$ slip is operated, slip on more than one system with $\bar{a}$ slip vector occurs and intersection of these screw dislocations produce jogs with edge character. These edge jogs can move only by non-conservative motion, that is by creation of point defects or by formation of dislocation loops. This accounts for the dislocation debris which is observed.

Twinning

Figure 8 shows optical micrographs of Ti-4Al tested at various cyclic strain amplitudes. It can be seen that many more twins are formed as the strain amplitude increases. The volume fraction of twins is plotted in Figure 10 as a function of applied strain amplitude for the Ti-4Al and Ti-8Al alloys. Even Ti-8Al exhibits some twinning during cyclic deformation although no twins are found in monotonic deformation. The reason for this may be the buildup of dislocation debris during cyclic deformation which makes continued deformation by slip difficult. Many fragmented twins, especially at higher strain amplitudes, also are noted.

## Summary and Conclusions

1) Cyclic deformation modes of Ti-Al alloys were found to be qualitatively

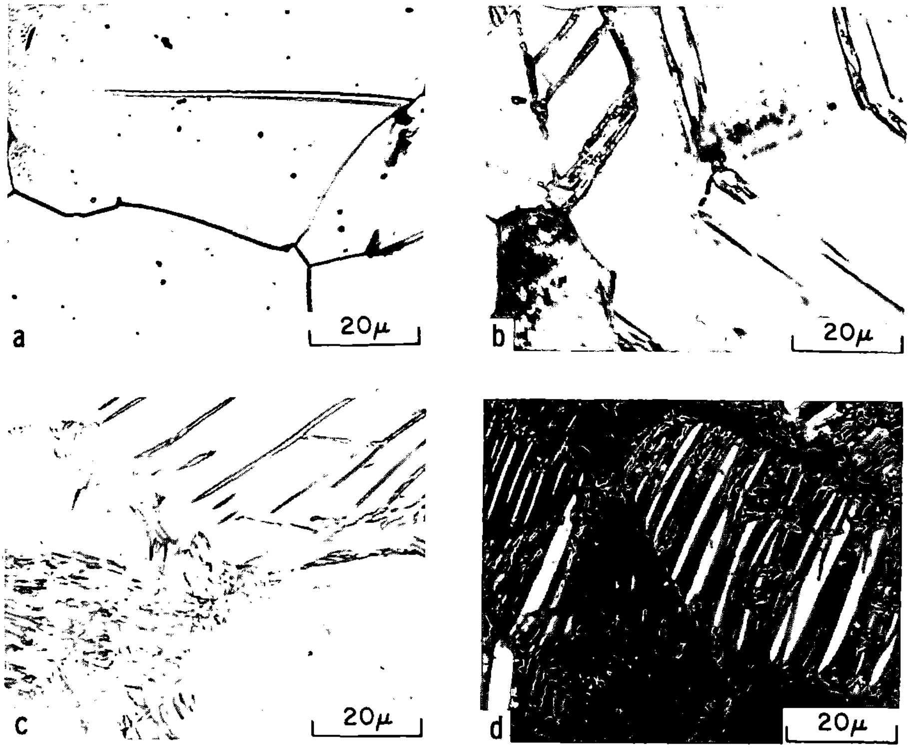


Fig. 8 - Twinning structures after cyclic deformation in Ti-4Al

a) $\frac{\Delta\varepsilon_T}{2} = 0.5\%$ b) $\frac{\Delta\varepsilon_T}{2} = 1\%$ c) $\frac{\Delta\varepsilon_T}{2} = 3\%$ d) $\frac{\Delta\varepsilon_T}{2} = 5\%$

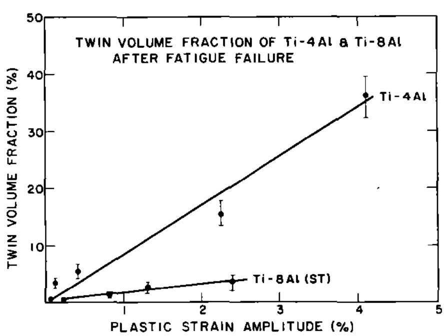


Fig. 9 - Caption is on figure.

similar to the monotonic deformation modes although the dislocation density is higher in cyclic deformation than after a corresponding amount of monotonic deformation.

2) The dominant deformation mode was $\bar{a}$ slip on prism planes in both monotonic and cyclic deformation.

3) The distribution of dislocations after cyclic deformation is comparable to that after the monotonically deformation at low strain amplitudes. As the strain amplitude is increased, poorly developed cellular structures are observed in Ti-4Al, whereas more closely spaced slip bands (tending toward homogeneous arrays) are seen in Ti-8Al.

4) Cyclic straining induces much more extensive dislocation debris than monotonic loading and most of dislocation debris has $\bar{a}$ Burgers Vector.

## Acknowledgments

This work has been supported by the Air Force Office of Scientific Research. Experimental work has been conducted using facilities provided by The Center for the Joining of Materials. The authors gratefully acknowledge the experimental assistance of M. Glatz and the secretarial help of Mrs. A. M. Crelli.

## References

1. N. E. Paton, J. C. Williams, and G. P. Rauscher: "The Deformation of α-Phase Titanium," Titanium Science and Technology, Vol. 2, p 1049, R. I. Jaffee and H. M. Burte, Eds., Plenum Press, (1973).
2. M. J. Blackburn and J. C. Williams: Trans. ASM, Vol. 62, (1969), 398.
3. D. J. Truax and C. J. McMahon, Jr.: Mater. Sci. Eng., Vol. 13, (1974), 125.
4. H. Rosenberg: Ph.D. Thesis, Stanford University (1971).
5. M. J. Blackburn and J. C. Williams: Trans. TMS-AIME, vol. 239, (1967), 287.
6. N. E. Paton, R. G. Baggerly, and J. C. Williams: Rockwell International Report, 1976.
7. J. C. Grosskreutz: Phys. Stat. Sol. (b) Vol. 47, (1971), 11.
8. W. T. Read: "Dislocations in Crystals," McGraw-Hill, 1953.

Table 1. Chemical compositions of Ti-4Al and Ti-8Al

| | Al | Fe | O | N |
|---|---|---|---|---|
| Ti-4Al | 3.91 | 0.053 | 0.06 | 0.011 |
| Ti-8Al | 8.0 | 0.050 | 0.08 | 0.011 |

Table 2. Twinning volume fractions of Ti-4Al and Ti-8Al

| Loading direction | Plastic strain($\varepsilon_p$) | Ti-4Al | Ti-8Al |
|---|---|---|---|
| Along the rolling axis (tension) | 0.3% | ∿ 0 | ∿ 0 |
| | 3.6% | 2% | 0 |
| Through thickness of plates (compression) | 3.6% | 3% | 0.5% |

Table 3. Monotonic slip characters

| Alloys | Applied plastic strain($\varepsilon_p$) | |
|---|---|---|
| | 0.3% | 3.6% |
| Ti-4Al | banded prism slip (some homogeneous $\bar{a}$ slip) | homogeneous $\bar{a}$ slip and twinning |
| Ti-8Al | banded prism slip | banded $\bar{a}$ slip |

Table 4. Cyclic slip characters

| Alloys | Applied total strain amplitudes $\frac{\Delta\varepsilon_T}{2}$ | | | |
|---|---|---|---|---|
| | 0.5% | 1% | 2% | >2% |
| Ti-4Al | homogeneous $\bar{a}$ slip | poorly developed cellular structures | poorly developed cellular structures | less cellular structures and high densities of dislocation debris and twins |
| Ti-8Al | few banded $\bar{a}$ slip | more banded slip | more homogeneous dislocation distribution | homogeneous dislocation distribution with high density |